ORNL/TM--11580

DE92 018150

Engineering Technology Division

ANALYSIS OF HYDRAULIC INSTABILITY OF ANS INVOLUTE FUEL PLATES

W. K. Sartory

Date Published - November 1991

Prepared by the
OAK RIDGE NATIONAL LABORATORY
Oak Ridge, Tennnessee 37831-6285
managed by
MARTIN MARIETTA ENERGY SYSTEMS, INC.
for the
U.S. DEPARTMENT OF ENERGY
under contract DE-AC05-84OR21400

DISCLAIMER

CONTENTS

ACRONYMS

ADINA	Automatic Dynamic Incremental Nonlinear Analysis
ANS	Advanced Neutron Source
CG	Complex General matrix eigenvalue solver
EISPACK	Eigensystems Package
HFIR	High Flux Isotope Reactor
PS-2	Physical Sciences No. 2 milestone reference core design

NOMENCLATURE

Lower-case Roman letters

a	inner radius of the involute (see Fig. 1)
b	outer radius of the involute (see Fig. 1)
ℓ_1, ℓ_2, ℓ_n	unit coordinate vectors directed along the α-axis, the z-axis, and normal to the midsurface, respectively
f	Fanning friction factor
g, g_m	weighting functions used for the orthogonality method of solution of the differential equations
h	fluid channel thickness
$\bar{h}$	unperturbed channel thickness
h_p	plate thickness
k	local involute curvature = $\frac{1}{r}$
ℓ	plate length
p	pressure in fluid acting on plate
r	local involute radius of curvature
t	time
u_1, u_2	plate deflection components in the directions tangential to the plate midsurface
v_1, v_2	fluid velocity components
v_u, v_d	fluid velocities upstream (u) and downstream (d) of a sudden expansion in channel cross section
v_M	Miller's critical velocity [see Eq. (21)]

w	plate deflection normal to the plate midsurface
z	axial coordinate measured downstream from the channel entrance

Upper-case Roman Letters

$[A]$	matrix of coefficients in the system of boundary condition equations [see Eq. (67)]
$[B]$	matrix of coefficients in the system of boundary condition equations [see Eq. (67)]
$[C]$	matrix developed from $[A]$ and $[B]$; $[C] = [B]^{-1}[A]$
D	plate bending stiffness [Eqs. (7)–(9)]
F	nondimensional fluid friction number = $2f\frac{\ell}{h}$
G	integral coefficient [see Eq. (63)]
K	plate-stretching stiffness [see Eqs. (4)–(6)]
L	nondimensional plate damping coefficient [see Eq. (30)]
$M_1, M_2, M_{12} = M_{21}$	plate bending and twisting moments
N	nondimensional density parameter [see Eq. (28)]
$N_1, N_2, N_{12} = N_{21}$	plate tensile and shear forces
Q_2	plate shear force directed normal to midsurface
R	plate aspect ratio = $\frac{\overline{\alpha}}{\ell}$
S	stability number; nondimensional unperturbed fluid velocity
T	nondimensional ratio of plate stretching to bending stiffness = $\overline{(\alpha)}^2 K/D$
W_n	plate deflection expansion coefficients [see Eq. (53)]

Greek letters

α	involute arc length running coordinate
$\overline{\alpha}$	total arc length of involute
β	axial wave number of perturbation [see Eq. (56)]
β_1, β_2	plate midsurface rotations
γ^0_{12}	plate midsurface shear strain
$\varepsilon^0_1, \varepsilon^0_2$	plate midsurface axial strains
ζ	eigenvalue of Eq. (68) = $i\beta$
κ_1, κ_2	plate midsurface bending curvatures due to perturbation
λ	plate damping coefficient [see Eqs. (1) - (3)]
ν	plate Poisson's ratio
ρ	fluid density
ρ_P	plate density
τ	plate midsurface twist due to perturbation
χ	eigenvector of Eq. (67)
θ, θ_n	expansion function for the plate normal deflection
ω	angular frequency of perturbation [see Eq. (56)]

Additional symbols

$'$	the prime is used with variables to indicate that they have been nondimensionalized
$\sim$	the tilde is used over the symbol for a variable to identify coefficients of $e^{i(\beta z' - \omega t')}$ [see Eq. (56)]

ACKNOWLEDGEMENTS

The author wishes to thank G. T. Yahr for his support of this work, C. R. Luttrell and R. C. Gwaltney for discussions of their earlier work in the same area, and W. F. Swinson for discussions of related experimental work. W. F. Swinson also performed a quality assurance review of the equation development, and C. R. Luttrell performed a quality assurance review of the computer program developed to carry out the calculations. W. R. Gambill, W. F. Swinson, and C. D. West reviewed this report.

ANALYSIS OF HYDRAULIC INSTABILITY OF ANS INVOLUTE FUEL PLATES

W. K. Sartory

ABSTRACT

Curved shell equations for the involute Advanced Neutron Source (ANS) fuel plates are coupled to two-dimensional hydraulic channel flow equations that include fluid friction. A complete set of fluid and plate boundary conditions is applied at the entrance and exit and along the sides of the plate and the channel. The coupled system is linearized and solved to assess the hydraulic instability of the plates.

---

1. INTRODUCTION

The Advanced Neutron Source[1] (ANS) is a highly enriched uranium fission reactor presently under design at the Oak Ridge National Laboratory to produce neutrons for research use. One primary objective is to achieve a high neutron flux. To meet this objective, a small reactor core with a high fission heating density is required, which leads the designers to seek high coolant velocities to remove the heat.

Since the work of Stromquist and Sisman in 1948,[2] it has been known that very high flow velocities past fuel plates can cause the plates to deform, buckle, and collapse. Excessive fuel plate deformation can impede coolant flow and heat removal and thus must be avoided in the reactor design.

An interesting explanation of the flow-induced buckling was proposed by Miller.[3] Miller coupled a plate deformation equation with Bernoulli's equation for the fluid. He argued that if a small perturbation (due to an initial plate imperfection or to any other

source) caused two adjacent plates to move closer together at some location, then the fluid velocity between them at that location would be increased. According to Bernoulli's equation, the fluid pressure between the plates would then drop, tending to force the plates even closer together. At a certain critical velocity, the fluid forces tending toward plate collapse would exceed the elastic forces tending to hold the plates in their design configuration, and the plates would buckle.

Miller studied both flat and uniformly curved cylindrical plates* with different boundary conditions along their supported edges. Patterned after the successful High Flux Isotope Reactor (HFIR),[4] the ANS will use fuel plates with an involute shape (see Fig. 1). Gwaltney and Luttrell[5] therefore extended Miller's theory to involute plates by coupling elastic finite-element models of the plates with Bernoulli's equation for the fluid. They found that the involute plates were much more stable than flat plates of the same span, because of the stiffening effect of their curvature, but not as stable as cylindrical plates with the same average curvature.

At the time of Miller's original work, it was immediately suspected that Bernoulli's equation might limit the accuracy of the stability predictions because it ignores fluid friction. Thus, Johansson[6] modified the fluid equation of the Miller model to include friction and found some effect on stability. Later analytical work by Scavuzzo[7] and by Smissaert[8] also included the effect of fluid friction on the Miller-type instability of flat plates.

---

*There is a conflict in terminology here. In solid mechanics, a plate is understood to be flat, and a curved plate is called a shell. In nuclear design practice, the term fuel plate is used regardless of curvature. In the present report, the curved involute fuel plates of the ANS and similar curved fuel plates of other reactors will be referred to either as plates or shells.

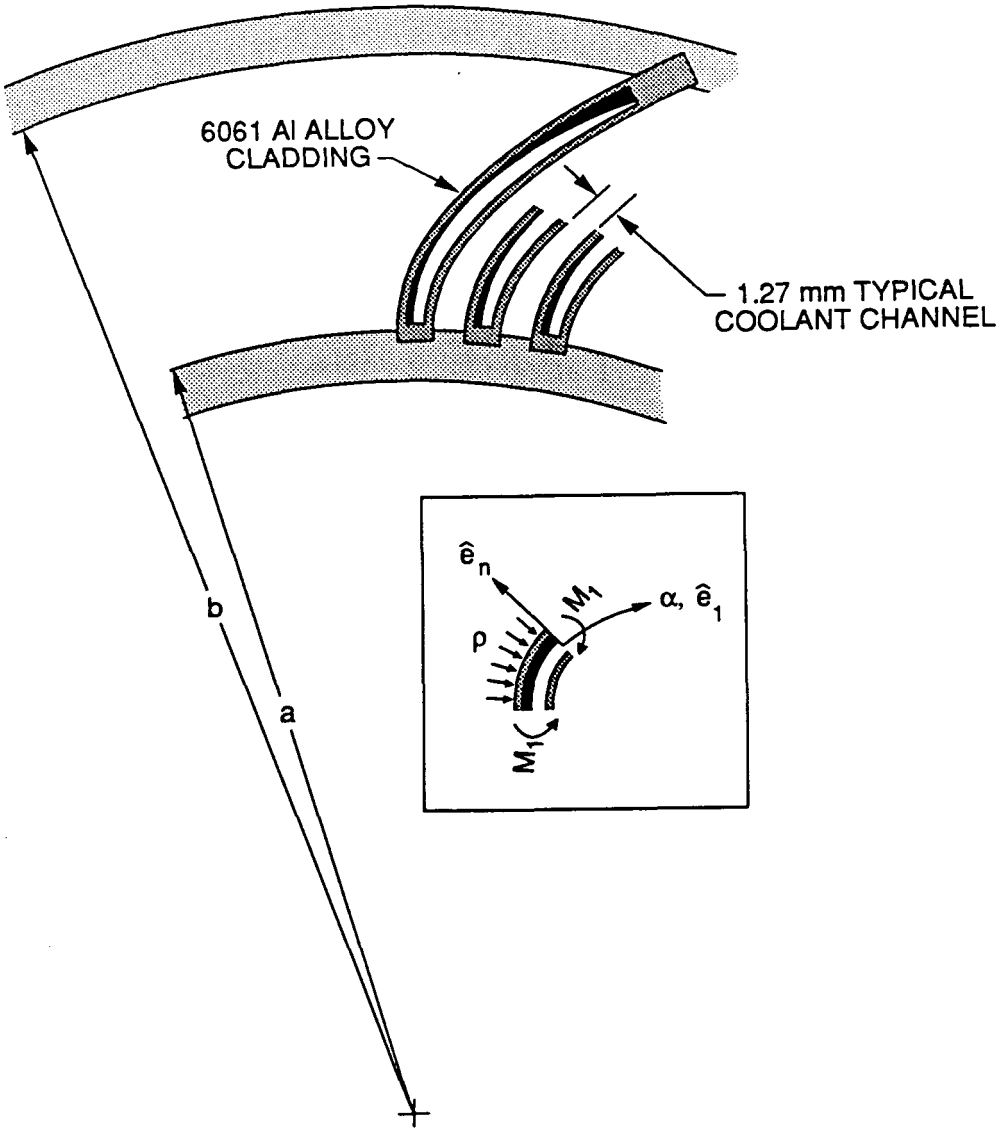

Fig. 1. Schematic representation of typical involute fuel plate. There is an array of several hundred involute plates in each of two assemblies in the PS-2 core. The side plate radii, *a* and *b*, are referred to in this report as the inner and outer radii of the involute, respectively. The inset shows the direction of the α axis, which is taken to be the first coordinate axis. The corresponding coordinate direction is shown by the unit vector $\hat{e}_1$. The second coordinate *z* and the second coordinate vector run into the page. The third coordinate direction is shown by the unit normal vector $\hat{e}_n$ in the inset. The curvature is positive when $\hat{e}_n$ points in the convex direction. A positive pressure loading p and a positive bending moment M_1 are also shown in the inset.

In the present analyses of Miller instability in the ANS, a linearized involute shell model of the fuel plates is coupled with a linearized hydraulic equation incorporating fluid friction to assess the allowable coolant flow velocity. Other changes compared with previous work include a fully two-dimensional (2-D) hydraulic model and the incorporation of both inlet and outlet fluid and plate boundary conditions. Inertial and damping terms (time derivatives) are also included in the fluid and plate equations, although computer cost limitations prevent the full utilization of the inertial terms. Incorporation of inertial terms and complete inlet and outlet boundary conditions allows the calculation of the normal modes of vibration of the coupled fluid-plate system under flow conditions. These vibrational modes and their associated frequencies and damping coefficients are of interest in the ANS design in their own right, in addition to their involvement in the Miller instability phenomenon.

2. EQUATIONS OF MOTION

Linearized shell equations using the approximations presented by Kraus[9] were used in the present work. After simplification to account for the fact that the involute fuel plates are curved only in one direction, these equations result:

$$\frac{\partial}{\partial \alpha}\left(\frac{\partial M_1}{\partial \alpha} + \frac{\partial M_{12}}{\partial z}\right) + \frac{\partial}{\partial z}\left(\frac{\partial M_{12}}{\partial \alpha} + \frac{\partial M_2}{\partial z}\right) - \frac{N_1}{r} =$$

$$-\left(-p - \lambda\frac{\partial w}{\partial t} - \rho_p h_p \frac{\partial^2 w}{\partial t^2}\right), \tag{1}$$

$$\frac{\partial N_1}{\partial \alpha} + \frac{\partial N_{21}}{\partial z} + \frac{1}{r}\left(\frac{\partial M_1}{\partial \alpha} + \frac{\partial M_{21}}{\partial z}\right) =$$

$$-\left(-\lambda\frac{\partial u_1}{\partial t} - \rho_p h_p \frac{\partial^2 u_1}{\partial t^2}\right), \tag{2}$$

$$\frac{\partial N_{12}}{\partial \alpha} + \frac{\partial N_2}{\partial z} = -\left(-\lambda\frac{\partial u_2}{\partial t} - \rho_p h_p \frac{\partial^2 u_2}{\partial t^2}\right), \tag{3}$$

$$N_1 = K\left(\varepsilon_1^0 + \nu\varepsilon_2^0\right), \tag{4}$$

$$N_2 = K\left(\varepsilon_2^0 + \nu\varepsilon_1^0\right), \tag{5}$$

$$N_{12} = N_{21} = K(1-\nu)\frac{\gamma_{12}^0}{2}, \tag{6}$$

$$M_1 = D\ (\kappa_1 + \nu\kappa_2)\ , \tag{7}$$

$$M_2 = D\ (\kappa_2 + \nu\kappa_1)\ , \tag{8}$$

$$M_{12} = M_{21} = D(1 - \nu)\tau/2\ , \tag{9}$$

$$\varepsilon_1^{\,0} = \frac{\partial u_1}{\partial \alpha} + \frac{w}{r}\ , \tag{10}$$

$$\varepsilon_2^{\,0} = \frac{\partial u_2}{\partial z}\ , \tag{11}$$

$$\gamma_{12}0 = \frac{\partial u_2}{\partial \alpha} + \frac{\partial u_1}{\partial z}\ , \tag{12}$$

$$\kappa_1 = \frac{\partial \beta_1}{\partial \alpha}\ , \tag{13}$$

$$\kappa_2 = \frac{\partial \beta_2}{\partial z}\ , \tag{14}$$

$$\tau = \frac{\partial \beta_2}{\partial \alpha} + \frac{\partial \beta_1}{\partial z}\ , \tag{15}$$

$$\beta_1 = \frac{u_1}{r} - \frac{\partial w}{\partial \alpha}\ , \tag{16}$$

$$\beta_2 = -\frac{\partial w}{\partial z} . \tag{17}$$

The variable α is the arc length coordinate measured around the midsurface of the involute plate starting at the inner radius of the involute (see Fig. 1); z is the axial coordinate starting at the inlet; t is time; M_1, M_2, and $M_{12} = M_{21}$ are plate bending and twisting moments; N_1, N_2, and $N_{12} = N_{21}$ are the tensile and shear forces; r (a function of α) is the unperturbed radius of curvature of the midsurface of the involute; p is the fluid pressure on the plate; w, u_1, and u_2 are the plate deflections; λ is a plate-damping coefficient; ρ_p is the plate density; h_p is the plate thickness; K is a plate-stretching stiffness; D is a plate-bending stiffness; ν is Poisson's ratio; ε_1^0, ε_2^0, and γ_{12}^0 are plate midsurface strains; β_1 and β_2 are plate midsurface rotations; and κ_1, κ_2, and τ are plate midsurface curvatures and twist in addition to the initial involute curvature. (At this stage in the equation development, there is just one fluid channel on one side of a single plate. Adjustments will be made later for the more interesting geometry of multiple plates with fluid channels on both sides of every plate.)

The 2-D nonlinear hydraulic equations (treating the channel as flat) are:

$$\frac{\partial \rho h}{\partial t} + \frac{\partial \rho h v_1}{\partial \alpha} + \frac{\partial \rho h v_2}{\partial z} = 0 , \tag{18}$$

$$\frac{\partial \rho h v_1}{\partial t} + \frac{\partial \rho h v_1^2}{\partial \alpha} + \frac{\partial \rho h v_1 v_2}{\partial z} = -h\frac{\partial p}{\partial \alpha} - f\rho(v_1^2 + v_2^2)^{1/2} v_1 , \tag{19}$$

$$\frac{\partial \rho h v_2}{\partial t} + \frac{\partial \rho h v_1 v_2}{\partial \alpha} + \frac{\partial \rho h v_2^2}{\partial z} = -h\frac{\partial \rho}{\partial z} - f\rho\left(v_1^2 + v_2^2\right)^{1/2} v_2 , \tag{20}$$

where ρ is the (constant) fluid density, h is the channel gap size, v_1 and v_2 are the fluid velocity components in the α and z directions, and f is the Fanning friction factor.

We now manipulate the equations in several ways. We eliminate many of the unknowns from the shell equations in favor of the three deflections. We linearize the hydraulic equations by perturbing about steady, uniform axial flow. We also nondimensionalize all of the equations. A natural choice of a velocity for nondimensionalization is the unperturbed axial fluid velocity, but we chose instead the Miller velocity:

$$v_M = \left[\frac{180D\bar{h}}{(\bar{\alpha})^4 \rho} \right]^{1/2}, \tag{21}$$

where $\bar{h}$ is the unperturbed channel thickness and $\bar{\alpha}$ is the total arc length of the involute. The Miller velocity is the critical velocity that would be calculated by Miller's theory for a flat plate with the same arc length as the involute plate. A system of six coupled partial differential equations results:

$$\frac{\partial v_1'}{\partial \alpha'} + R \frac{\partial v_2'}{\partial z'} - 2'SR \frac{\partial w'}{\partial z'} - 2'RN \frac{\partial w'}{\partial t'} = 0, \tag{22}$$

$$RS\frac{\partial v_2'}{\partial z'} + RN\frac{\partial v_2'}{\partial t'} = - SRFv_2' - \frac{1}{2} R\frac{\partial p'}{\partial z'} - \frac{1}{2} 2'S^2RFw', \tag{23}$$

$$SR \frac{\partial v_1'}{\partial z'} + RN\frac{\partial v_1'}{\partial t'} = - \frac{1}{2}SRFv_1' - \frac{1}{2} \frac{\partial p'}{\partial \alpha'}, \tag{24}$$

$$\frac{\partial^3 k'}{\partial \alpha'^3} u_1' - Tk'^2 w' - \nu RTk' \frac{\partial u_2'}{\partial z'} - Tk' \frac{\partial u_1'}{\partial \alpha'} + R^2 k' \frac{\partial^3 u_1'}{\partial \alpha' \partial z'^2}$$

$$+ k' \frac{\partial^3 u_1'}{\partial \alpha'^3} + R^2 \frac{\partial k'}{\partial \alpha'} \frac{\partial^2 u_1'}{\partial z'^2} - 2R^2 \frac{\partial^4 w'}{\partial z'^2 \partial \alpha'^2} - R^4 \frac{\partial^4 w'}{\partial z'^4} + 3 \frac{\partial^2 k'}{\partial \alpha'^2} \frac{\partial u_1'}{\partial \alpha'}$$

$$+ 3 \frac{\partial k'}{\partial \alpha'} \frac{\partial^2 u_1'}{\partial \alpha'^2} - \frac{\partial^4 w'}{\partial \alpha'^4} = 90 \times 2' 'p' + L \frac{\partial w'}{\partial t'} + \frac{\partial^2 w'}{\partial t'^2}, \qquad (25)$$

$$k' \frac{\partial^2 k'}{\partial \alpha'^2} u_1' + T \frac{\partial k'}{\partial \alpha'} w' + Tk' \frac{\partial w'}{\partial \alpha'} - R^2 k' \frac{\partial^3 w'}{\partial \alpha' \partial z'^2} + 2 \frac{\partial k'}{\partial \alpha'} k' \frac{\partial u_1'}{\partial \alpha'}$$

$$- k' \frac{\partial^3 w'}{\partial \alpha'^3} + \nu RT \frac{1}{2} \frac{\partial^2 u_2'}{\partial \alpha' \partial z'} - \nu R^2 T \frac{1}{2} \frac{\partial^2 u_1'}{\partial z'^2}$$

$$+ RT \frac{1}{2} \frac{\partial^2 u_2'}{\partial \alpha' \partial z'} + T \frac{\partial^2 u_1'}{\partial \alpha'^2} - \nu R^2 \frac{1}{2} k'^2 \frac{\partial^2 u_1'}{\partial z'^2} + k'^2 \frac{1}{2} R^2 \frac{\partial^2 u_1'}{\partial z'^2}$$

$$+ k'^2 \frac{\partial^2 u_1'}{\partial \alpha'^2} + R^2 T \frac{1}{2} \frac{\partial^2 u_1'}{\partial z'^2} = L \frac{\partial u_1'}{\partial t'} + \frac{\partial^2 u_1'}{\partial t'^2}, \qquad (26)$$

$$\nu RTk' \frac{\partial w'}{\partial z'} + \nu RT \frac{1}{2} \frac{\partial^2 u_1'}{\partial \alpha' \partial z'} - \nu T \frac{1}{2} \frac{\partial^2 u_2'}{\partial \alpha'^2} + RT \frac{1}{2} \frac{\partial^2 u_1'}{\partial \alpha' \partial z'} + T \frac{1}{2} \frac{\partial^2 u_2'}{\partial \alpha'^2}$$

$$+ R^2 T \frac{\partial^2 u_2'}{\partial z'^2} = L \frac{\partial u_2'}{\partial t'} + \frac{\partial^2 u_2'}{\partial t'^2} \qquad (27)$$

The variables v_1' and v_2' are the fluid velocity perturbations nondimensionalized with v_M, $\alpha' = \alpha/\bar{\alpha}$, $z' = z/\ell$, ℓ is the total length of the channel, $R = \bar{\alpha}/\ell$, $2'$ is a factor of 2 introduced into Eqs. (22) and (23) to account for the change from a single plate to an array of plates in which adjacent plates deflect in opposite directions so that the perturbation in channel thickness is twice the plate deflection, $2''$ is a factor of 2 introduced into Eq. (25) to account for the fact that a fluid channel with a pressure perturbation is present on both sides of the plate, S is the unperturbed fluid velocity divided by v_M and will be called the stability number, w' is the plate normal deflection divided by $\bar{h}$, p' is the fluid pressure perturbation divided by $\frac{1}{2}\rho v_M 2$, $k' = \bar{\alpha}/r$ is the involute nondimensionalized unperturbed curvature, u_1' and u_2' are the plate tangential deflections divided by $\bar{h}$, $T = (\bar{\alpha})^2 K/D$, $F = 2f\,\ell/\bar{h}$ is the fluid friction number,

$$N = \left(\frac{\rho}{180\rho_p}\right)^{1/2} \frac{\ell}{\bar{h}}, \tag{28}$$

$$t' = \frac{t}{(\bar{\alpha})^2 \left(\frac{h_p \rho_p}{D}\right)^{1/2}}, \tag{29}$$

$$L = \frac{(\bar{\alpha})^2 \lambda}{\left(h_p \rho_p D\right)^{1/2}}. \tag{30}$$

The nondimensional curvature function can be shown to be

$$k'(\alpha') = \frac{1}{2}\left[\left(\frac{b}{a}\right)^2 - 1\right]^{1/2} \alpha'^{-1/2}, \tag{31}$$

where a is the inner radius of the involute and b is the outer radius (see Fig. 1).

Along the built-in sides of the plate, the boundary conditions are

$$w' = \frac{\partial w'}{\partial \alpha'} = u_1' = u_2' = 0, \tag{32}$$

and along the sides of the channel

$$v_1' = 0, \tag{33}$$

at $\alpha' = 0$ and 1.

Along the leading and trailing edges of the plate, there are assumed to be no concentrated forces or moments. There appears to be five edge forces and moments that can be set to zero at such an edge:

$$N_2 = 0, \tag{34}$$

$$N_{21} = 0, \tag{35}$$

$$M_2 = 0 , \tag{36}$$

$$M_{21} = 0 , \tag{37}$$

$$Q_2 = 0 , \tag{38}$$

where Q_2 is the shearing force per unit length of edge directed normal to the midsurface of the shell. It is known,[9] however, that only four independent conditions can be set.

$$N_2 = 0 , \tag{39}$$

$$N_{21} + \frac{M_{21}}{r} = 0 , \tag{40}$$

$$Q_2 + \frac{\partial M_{21}}{\partial \alpha} = 0 , \tag{41}$$

$$M_2 = 0 . \tag{42}$$

The shear force Q_2 may be eliminated using the equilibrium equation[9]

$$Q_2 = \frac{\partial M_{21}}{\partial \alpha} + \frac{\partial M_2}{\partial z} \tag{43}$$

to give

$$2\frac{\partial M_{21}}{\partial \alpha} + \frac{\partial M_2}{\partial z} = 0 \tag{44}$$

in place of Eq. (41). Eliminating the unknowns from the boundary conditions in favor of the displacements and nondimensionalizing,

$$\nu k' w' + R\frac{\partial u_2'}{\partial z'} + \nu\frac{\partial u_1'}{\partial \alpha'} = 0 , \tag{45}$$

$$k'(2-2\nu)R\,\frac{\partial^2 w'}{\partial \alpha' \partial z'} + T\left[(\nu - 1)\frac{\partial u_2'}{\partial \alpha'} + R(\nu - 1)\frac{\partial u_1'}{\partial z'}\right] + k'^2 R(\nu - 1)\frac{\partial u_1'}{\partial z'} = 0 , \tag{46}$$

$$-R^2\frac{\partial^3 w'}{\partial z'^3} + (\nu - 2)\frac{\partial^3 w'}{\partial \alpha'^2 \partial z'} + \frac{\partial k'}{\partial \alpha'}\frac{\partial u_1'}{\partial z'} + k'\frac{\partial^2 u_1'}{\partial \alpha' \partial z'} = 0 , \tag{47}$$

$$-R^2\frac{\partial^2 w'}{\partial z'^2} - \nu\frac{\partial^2 w'}{\partial \alpha'^2} + \nu k'\frac{\partial u_1'}{\partial \alpha'} + \nu\frac{\partial k'}{\partial \alpha'}u_1' = 0 , \tag{48}$$

at $z' = 0$ and 1. At the channel entrance ($z' = 0$), the pressure perturbation is related to the velocity perturbation,

$$p' + 2(1 + C_e)S\nu_2' = 0 , \tag{49}$$

where C_e is an entrance contraction loss coefficient that we shall take as 0.04* for rounded plate leading edges with a radius of $h_p/2$.

We assume that the inlet flow is guided straight into the channel by ducting or vanes, so

$$v_1' = 0 \tag{50}$$

at the entrance ($z' = 0$). The channel exit condition requires further discussion.

At a sudden expansion in channel cross section, the Borda-Carnot equation[10] is usually recommended without any correction:

$$\text{static pressure rise} = \frac{1}{2}\rho(v_u^2 - v_d^2) - \frac{1}{2}\rho(v_u - v_d)^2 , \tag{51}$$

where v_u is the upstream velocity and v_d is the downstream velocity. Associated with this equation, however, is a standard derivation.[10] A fundamental assumption of the derivation is that at a channel section located an infinitesimal distance downstream of the expansion, the fluid pressure is uniform across the section, and that the fluid pressure in the upstream channel drops (due to fluid friction) smoothly to the section pressure at the expansion section. This assumption allows the Borda-Carnot equation to be obtained by momentum balance. Borda's assumption is also the basis of the theory of jet pumps and ejectors in which two fluid streams traveling at different velocities are introduced into a common channel. In

*For turbulent flow, Vennard[11] recommends $C_e = 0.04$ when the entrance is rounded with a radius of curvature ≥0.15 of the channel equivalent diam. However, Hobbs[12] recommends $C_e = 0$ when the entrance radius is ≥0.13 of the channel equivalent diam. The ANS is expected to use a plate-leading edge radius equal to 0.25 channel equivalent diameters (0.5 h_p).

the present work, we apply the fundamental Borda assumption of uniform pressure to two adjacent upstream channels of the involute exit. Then the pressure in each of the upstream channels extrapolates smoothly to the same common pressure at the expansion. Because the pressure perturbation is assumed to have opposite signs in adjacent channels,

$$p' = 0, \tag{52}$$

at the exit ($z' = 1$).

Because the upstream contraction loss coefficient value of 0.04 does not seem very definitely established in the literature [11,12] and because no other authors have used Borda's assumption in the above way to get the downstream boundary condition, it seems worth noting here that numerical experiments performed during the present work indicate that for the involute plate studied, a change from the present boundary conditions to the lossless Bernoulli's equation at the entrance and exit causes at most roughly a 10% change in the calculated stability number.

If all solutions of the boundary value problem Eqs. (22)-(27), (32)-(50), and (52) decay in time, then the plate is stable. If any solution grows in time, then the plate is unstable. The calculated critical value of the stability number is the value on the boundary between stable and unstable regimes. The calculated critical stability number is generally a function of the other nondimensional parameters: R,F,T,N,L, and the radius ratio of the involute that determines the curvature function $k'(\alpha')$.

3. SOLUTION ALGORITHM

The coefficients of the linear partial differential Eqs. (22)–(27) and (32)–(52) are independent of t' and z' but depend on α' through the curvature function k'. In the present work, we use the orthogonality method[13] to treat the α'-dependence. Each of the unknown functions is expanded in a series of coordinate functions of α'; for example,

$$w'(t',z',\alpha') = \sum_{n=1}^{6} w_n\,(t',z')\phi_n(\alpha') \,, \tag{53}$$

where each coordinate function, $\phi_n(\alpha')$, satisfies all required side boundary conditions on w', and similarly for the other five unknowns. The use of a six-term series is, of course, somewhat arbitrary. Other numbers of terms were also tried, as will be discussed later. After substituting all such expansions into the differential equations, each differential equation is multiplied by a sequence of weighting functions of $\alpha', g_m(\alpha')$ and integrated with respect to α' from 0 to 1. This procedure leads to a system of partial differential equations with constant coefficients in the independent variables t' and z' in which α' is eliminated as an independent variable.

In the present work, polynominals were used both for the expansion functions and for the weight functions. For example, the first expansion function for w' was the same function used by Miller for flat plates:

$$\phi_1(\alpha') = \alpha'^2(1 - \alpha')^2 \,. \tag{54}$$

The higher expansion functions were higher degree polynominals of the same general form. The weight functions used to weight the shell deflection [Eq. (25)] were taken to be the same as the expansion functions for w

$$g_m(\alpha') = \phi_m(\alpha'), \; m = 1 \text{ thru } 6. \tag{55}$$

Similar expansion and weight functions (satisfying different boundary conditions) were used for the other variables and equations.

We then seek solutions of Eqs. (22) - (27) in the form

$$W_n(t', z') = \bar{w}_n e^{i(\beta z' - \omega t')}, \tag{56}$$

and similarly for the other unknowns. The result of the substitution is a system of linear algebraic equations for the unknowns $\bar{w}_n$ etc.:

$$G(1,1,1,0)\bar{v}_1 + RG(1,2,0,0)i\beta\bar{v}_2 - 2'SRG(1,4,0,0)i\beta\bar{w}$$

$$- 2'RNG(1,4,0,0)\,(-i\omega)\bar{w} = 0, \tag{57}$$

$$RSG\,(2,2,0,0)i\beta\bar{v}_2 + RNG(2,2,0,0)\,(-i\omega)\bar{v}_2$$

$$= - SRFG(2,2,0,0)\bar{v}_2 - \frac{1}{2}RG(2,3,0,0)i\beta\bar{p} - \frac{1}{2}2'S^2RFG(2,4,0,0)\bar{w}, \tag{58}$$

$$SRG(3,1,0,0)i\beta\bar{v}_1 + RNG(3,1,0,0)(-i\omega)\bar{v}_1$$

$$= -\frac{1}{2} SRFG(3,1,0,0)\bar{v}_1 - \frac{1}{2} G(3,3,1,0)\bar{p} , \tag{59}$$

$$G(4,5,0,5)\bar{u}_1 - TG(4,4,0,2)\bar{w} - \nu RTG(4,6,0,1)i\beta\bar{u}_2$$

$$- TG(4,5,1,1)\bar{u}_1 + R^2G(4,5,1,1)(-\beta^2)\bar{u}_1 + G(4,5,3,1)\bar{u}_1$$

$$+ R^2G(4,5,0,3)(-\beta^2)\bar{u}_1 - 2R^2G(4,4,2,0)(-\beta^2)\bar{w} - R^4G(4,4,0,0)\beta^4\bar{w}$$

$$+ 3G(4,5,1,4)\bar{u}_1 + 3G(4,5,2,3)\bar{u}_1 - G(4,4,4,0)\bar{w}$$

$$= 90 \times 2''G(4,3,0,0)\bar{p} + TG(4,4,0,0)(-i\omega)\bar{w} + G(4,4,0,0)(i\omega)^2\bar{w} , \tag{60}$$

$$G(5,5,0,7)\bar{u}_1 + TG(5,4,0,3)\bar{w} + TG(5,4,1,1)\bar{w}$$

$$- R^2G(5,4,1,1)(i\beta)^2\bar{w} + 2G(5,5,1,6)\bar{u}_1 - G(5,4,3,1)\bar{w}$$

$$+ \nu RT\frac{1}{2}G(5,6,1,0)i\beta\bar{u}_2 - R^2\nu T\frac{1}{2}G(5,5,0,0)(i\beta)^2\bar{u}_1$$

$$+ RT\frac{1}{2}G(5,6,1,0)i\beta\bar{u}_2 + TG(5,5,2,0)\bar{u}_1$$

$$- \nu R^2 \frac{1}{2} G(5,5,0,2)(i\beta)^2 \bar{u}_1 + R^2 \frac{1}{2} G(5,5,2,0) \bar{u}_1$$

$$+ G(5,5,2,2) \bar{u}_1 + R^2 T \frac{1}{2} G(5,5,0,0)(i\beta)^2 \bar{u}_1$$

$$= LG(5,5,0,0)(-i\omega) \bar{u}_1 + G(5,5,0,0)(i\omega)^2 \bar{u}_1 , \tag{61}$$

$$\nu RTG(6,4,0,1) i\beta \bar{w} + \nu RT \frac{1}{2} G(6,5,1,0) i\beta \bar{u}_1$$

$$- \nu T \frac{1}{2} G(6,6,2,0) \bar{u}_2 + RT \frac{1}{2} G(6,5,1,0) i\beta \bar{u}_1$$

$$+ T \frac{1}{2} G(6,6,2,0) \bar{u}_2 + R^2 TG(6,6,0,0)(i\beta)^2 \bar{u}_2$$

$$= LG(6,6,0,0)(-i\omega) \bar{u}_2 + G(6,6,0,0)(i\omega)^2 \bar{u}_2 . \tag{62}$$

The G's are quadratures involving the expansion functions or their derivatives, the weighting functions, and the curvature function in various forms.

The first argument of G is the equation index that runs from 1 to 6, referring to Eqs. (57–62), respectively.

The second argument of G is the unknown index that also runs from 1 to 6. For purposes of the second argument of G, the unknowns are arranged in the order: $\bar{v}_1$, $\bar{v}_2$, $\bar{p}$, $\bar{w}$, $\bar{u}_1$, $\bar{u}_2$.

The third argument of G is a derivative order index on the expansion function that runs from 0 to 4.

The fourth argument of G refers to the way in which the curvature function appears in the quadrature. It runs from 0 to 7 and is defined as follows.

Fourth argument	Curvature function
0	1.0
1	k'
2	k'^2
3	$\frac{dk'}{d\alpha'}$
4	$\frac{d^2k'}{d\alpha'^2}$
5	$\frac{d^3k'}{d\alpha'^3}$
6	$k'\frac{dk'}{d\alpha'}$
7	$k'\frac{d^2k'}{d\alpha'^2}$

As an example,

$$G(4,1,1,1) = \int_0^1 g(\alpha)k'(\alpha') \frac{d\phi(\alpha)}{d\alpha'} d\alpha' . \tag{63}$$

The G's were evaluated numerically by Gaussian quadrature.

In addition to the four explicit indices expressed as arguments of G, there are also two implied indices [the expansion index n from Eq. (53) and the weight index m on g] that are suppressed in the equations to reduce the clutter. The expansion index n also appears on each of the unknowns [as in Eq. (53)]. The summation convention is understood to apply to n and the range convention is understood to apply to m. If n and m run from 1 to 6 (the usual choice for most of the numerical work in this report), then there are six times as many unknowns and six times as many equations as appear explicitly in Eqs. (57)–(62).

The parameter β (the axial wave number of the perturbation) appears in Eqs. (57)–(62) with powers from 0 to 4. We now restrict its appearance to the powers 0 and 1 by introducing additional unknowns. For example, we define

$$\bar{w}_1 = i\beta\bar{w} , \tag{64}$$

$$\bar{w}_2 = i\beta\bar{w}_1 , \tag{65}$$

$$\bar{w}_3 = i\beta\bar{w}_2 , \tag{66}$$

and similarly we define one subsidiary variable associated with each of $\bar{u}_1$ and $\bar{u}_2$ by introducing another index to eliminate powers of β. This substitution leads to five additional unknowns. To obtain five additional equations, we supplement the system Eqs. (57)–(62) by

Eqs. (64)–(66) and by the similar equations associated with $\bar{u}_1$ and $\bar{u}_2$. The system then contains (explicitly) 11 unknowns and 11 equations. Taking into account the suppressed indices, it contains 66 unknowns and 66 equations. After the appearance of β has been restricted to powers 0 and 1, we move all terms involving β^0 to the left-hand side and all terms involving β^1 to the right-hand side. That leads to an eigenvalue problem of the form

$$[A]\mathbf{x} = \zeta[B]\mathbf{x}\,, \tag{67}$$

where $[A]$ and $[B]$ are square, complex, non-Hermitian matrices, $\zeta = i\beta$ is the complex eigenvalue, and $\mathbf{x}$ is a column vector of the unknowns of Eqs. (57)–(62) supplemented by the new unknowns introduced to eliminate high powers of β. If n and m run from 1 to 6, then $[A]$ and $[B]$ are 66 x 66 matrices. Multiplying Eq. (67) from the left by the inverse of $[B]$, we obtain the standard form

$$[C]\mathbf{x} = \zeta\mathbf{x}\,. \tag{68}$$

The eigenvalue problem Eq. (68) was solved in the present work with the standard EISPACK[14] subroutine named CG*.

*Although CG is an implementation of an old and highly respected algorithm, problems were nevertheless occasionally encountered with it in the present work. These problems always were associated with multiple eigenvalues. If a matrix possesses a complete set of eigenvectors associated with a set of multiple eigenvalues, it is possible to define the eigenvectors so that they are mutually orthogonal. However, CG does not do this. Occasionally, the eigenvectors returned by CG for multiple eigenvalues were so far from orthogonality that, from a numerical point of view, they were not linearly independent. It was first believed that this result might indicate that the matrix $[C]$ was deficient (lacked a complete set of eigenvectors). However, the CG algorithm was then modified for multiple eigenvalues to use repeated inverse iteration followed by Gram-Schmidt orthogonalization to recalculate the eigenvectors. The vectors generated in this way were tested by direct substitution into Eq. (68) and were found to be genuine eigenvectors and also to be orthogonal and therefore linearly independent. It is concluded that CG, although old, is still unnecessarily unreliable in the special case of multiple eigenvalues.

The solutions (usually 66) of the special form of Eq. (56) obtained from the solution of the eigenvalue problem must be superimposed to satisfy the upstream and downstream edge-boundary conditions. The boundary conditions cannot be satisfied exactly by the present approximate solution and are instead satisfied approximately in the sense of the orthogonality method, just as the differential equations are satisfied in the orthogonality sense. For each of the 11 boundary conditions, we form a series solution with unknown coefficients. Then we multiply each boundary condition by one of six weighting functions and integrate with respect to α' from 0 to 1 to obtain a set of 66 homogeneous, linear algebraic equations for the coefficients. For a solution to exist, the determinant of the equations must be (complex) zero. If a value of the complex frequency ω is found for which the complex determinant is zero, then ω gives the frequency and decay rate of a normal vibrational mode, and the corresponding coefficients give the mode shape. Muller's method[15] has been used to calculate the complex frequencies.

The most reliable method of approaching coupled fluid-solid stability problems[16] seems to be to choose a number of normal vibrational modes (those of lowest real frequency) and to follow their complex frequencies from a fluid velocity of zero where stability is assumed to every-increasing fluid velocities until the first mode becomes unstable (the first root crosses from the negative imaginary half plane to the positive imaginary half plane or the corresponding decay rate changes from positive to negative). Even if such an approach is followed, it cannot be proven on the basis of numerical calculations that some mode higher than those studied does not become unstable first. In the present work, a large number of modes were followed during a preliminary phase of the investigation that was confined to flat fuel plates. It was found that the instability corresponded to monotonic collapse (divergence)

of the plate rather than to unstable flutter; that is, the complex frequency crossed from the negative to the positive imaginary half plane by passing through the origin.

In the later stages of this work that were devoted to involute plates, the computational cost of following a large number of normal modes from zero coolant velocity to the point of instability seemed prohibitive. Therefore, it was assumed that instability of involute plates also occurred by monotonic collapse (consistent with the theory of Miller and the work of all previous investigators of hydraulic instability). The complex frequency was set to (complex) zero, and the stability number (the nondimensional coolant velocity) was incremented gradually from a small value until the determinant (which was real to numerical precision) changed sign. The critical value of the stability number was then taken to lay in the interval that contained the sign change.

4. NUMERICAL RESULTS

The computational method described has been applied to the ANS core designs and to other experimental geometries.

The ANS core design is still evolving. In January 1989, a tentative two-part core design, PS-2, was developed that used two sets of involute plates with different radii. The inner subcore had these nominal dimensions and properties:

inner involute radius	=	102 mm
outer involute radius	=	168 mm
involute arc length	=	87.35 mm
plate length	=	494 mm
plate thickness	=	1.27 mm
plate density	=	3390 kg/m^3 (with estimated fuel)
coolant gap thickness	=	1.27 mm
coolant density	=	1096.65 kg/m^3
coolant viscosity	=	6.51×10^{-4} Pa · s
plate elastic modulus	=	6.89×10^{10} Pa
Poisson's ratio	=	0.33
coolant velocity	=	51.4 m/s*
λ	=	0†

*The design coolant velocity for PS-2 was 27.4 m/s. With the design margin of 0.8/1.5 included, the plates must be stable up to 51.4 m/s.

†The amount of plate solid damping is not known at this time, but overall damping is believed to be dominated by fluid dissipation.

The following nondimensional parameters are then obtained:

$$F = 2.98$$

$$R = 0.177$$

$$T = 56{,}767$$

$$N = 16.49$$

$$\frac{b}{a} = 1.647$$

$$L = 0$$

Some results of stability calculations are represented in Fig. 2 as a plot of the calculated stability number vs the fluid friction number F. Recall that the stability number is the ratio of the critical fluid velocity to the critical velocity that would be calculated by Miller's equation for a flat channel of the same arc length. In addition to the PS-2 inner core results, the stability number for flat fuel plates ($b/a = 1.0$) with the same arc length and the same other nondimensional parameters as the PS-2 design is also shown for comparison.

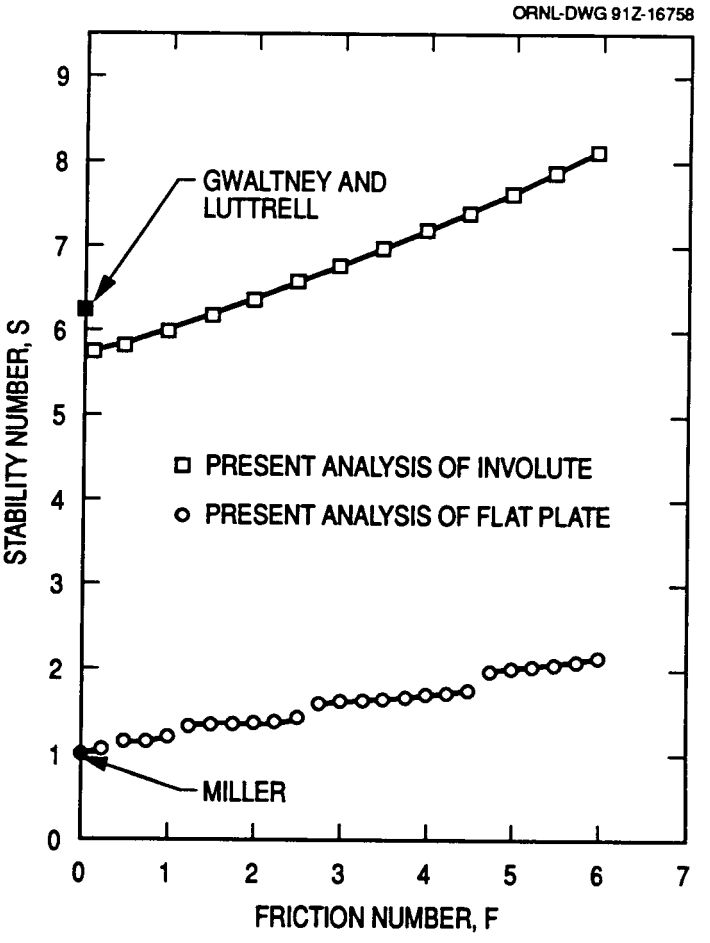

Fig. 2. Effect of fluid friction on hydraulic instability of fuel plates of ANS PS-2 geometry.

5. DISCUSSION OF RESULTS

The lower curve of Fig. 2 for flat plates shows that, as the fluid friction is reduced to zero, the critical stability number calculated by the present algorithm goes essentially to 1.0 in agreement with the frictionless theory of Miller.[3] As the fluid friction number is increased, the calculated stability number increases. The increase is significant and exceeds a factor of 2 at a friction number of 5 or 6. The theory of Johannson,[6] which included fluid friction, also predicts some effect on calculated stability; however, the effect predicted by Johannson depends on assumptions that must be made about the shape of the plate deflection perturbation occurring. The present theory, which calculates and uses the shape of the most unstable eigenfunction of the fluid-plate system, gives an unqualified prediction of the friction effect.

The lower curve is not smooth but comprises a series of segments. These different segments are believed to be associated with different axial modes of the marginally stable disturbance. These mode shifts deserve further study because such transitions are sometimes associated with the appearance of the oscillatory or flutter form of instability. The study of oscillatory modes, however, is beyond the scope of the present work.

The upper curve of Fig. 2 applies to PS-2 inner core involute plates. At small values of F, it is a factor of ~6 higher than the curve for flat plates because of the stiffening effect of the curvature (recall that the stability number of the present work is nondimensionalized by dividing the critical velocity by the flat plate Miller velocity).

The upper curve also shows an improvement in the calculated stability with increasing fluid friction number; however, on a percentage basis, the friction effect is much less than

with flat plates. At the PS-2 nominal friction number of 2.98, the calculated stability number is ~6.75, which corresponds to a dimensional calculated critical velocity of ~46.5 m/s. The PS-2 inner subcore plates at the design velocity of 27.4 m/s would then be operating at ~59% of their calculated maximum stable velocity, which is just beyond the target design margin of 0.8/1.5. As the friction number goes to zero, the present involute calculations differ (by <10%) from the frictionless calculated results of Gwaltney and Luttrell.[5] This difference is believed to be due to the difference in fluid boundary conditions used. It is not known at this time why the involute curve of Fig. 2 is smooth whereas the flat plate curve comprises several distinct segments.

As seen from Eq. (31), the curvature of a mathematically perfect involute has a singularity at the origin of the involute. Of course, real formed plates cannot have an infinite curvature at the origin, and the actual target shape for the forming process differs slightly near the origin from the mathematical involute. Although the singularity is a mathematical fiction, the question still arises as to whether slight deviations from the singularity have a large effect on the stability of real plates and also whether such slight deviations have a large effect on this and other computational algorithms. Luttrell[17] has studied the effect of a small change in the shape of the plates near the origin of the involute using the ADINA[18] finite-element program and has concluded that there was little effect on the predictions of the Gwaltney-Luttrell[5] stability algorithm. In the present work, the quadratures involving the curvature function have been performed using Gauss-Legendre integration. This method uses nodes that exclude the origin and is exact for certain interpolation polynominals. The interpolation polynominals are never singular. Thus, the results of this work might be interpreted as applying to plates with a nonsingular polynominal curvature shape that

approximates the involute shape to a varying degree depending on the number of nodes chosen. The sensitivity of the present method has been studied by repeating the calculations using differing numbers of Gaussian nodes (which approach the origin by differing distances). No unusual sensitivity of the calculated critical stability number to changes in the number of the Gaussian nodes or in their proximity to the origin was noted.

Most of the calculations of the present work were performed using a six-term expansion, Eq. (53), for each unknown function. A few exploratory calculations were also made with fewer terms. These indicate that four terms are usually adequate. Four terms are needed to approximate the rather complicated deflection shape taken by the involute under load. The hydraulic equations are believed to require only one term. Numerical experiments on flat plates show that only one term is needed for the geometry for both the plate equation and the hydraulic equation. It is likely that if the first term of the involute plate deflection equation were specifically chosen to represent the deflection shape of the involute under uniform pressure load, then a one-term series for both the plate and hydraulic equations would be adequate for the involute geometry, too. A great savings in computing time and in storage requirements over the present work would then result.

6. SUMMARY

A technique has been developed for analyzing the hydraulic instability of ANS fuel plates of involute shape. Fluid friction is included in the analysis. Fluid and plate entrance and exit and side-boundary conditions are applied, and normal vibrational modes of the fluid-plate system are calculated. As the fluid velocity is increased, in most cases the first vibrational mode becomes unstable only after its frequency drops to zero as discussed by Miller,[3] so the instability takes the form of a monotonic collapse rather than a flutter of growing amplitude. There is some indirect evidence, however, that unstable flutter might occur first for very short plates (length less than span).

Under ANS flow conditions, fluid friction increases the calculated critical velocity by ~17%. The effect of fluid friction is calculated to be much greater on a percentage basis for flat plates.

REFERENCES

1. G. L. Copeland et al., *Advanced Neutron Source Final Preconceptual Reference Core Design*, ORNL/TM-11234, Martin Marietta Energy Systems, Inc., Oak Ridge Natl. Lab., August 1989.

2. W. K. Stromquist and O. Sisman, *High Flux Reactor Fuel Assemblies Vibration and Water Flow*, ORNL-50, Oak Ridge Natl Lab., June 1948.

3. D. R. Miller, "Critical Flow Velocities for Collapse of Reactor Parallel-Plate Fuel Assemblies," *J. Eng. Power, Trans ASME*, 83–95, April 1960.

4. F. T. Binford and E. N. Cramer, *The High Flux Isotope Reactor, Volume I, Functional Description*, ORNL-3572, Union Carbide Corp., Nuclear Div., Oak Ridge Natl. Lab., May 1964.

5. R. C. Gwaltney and C. R. Luttrell, "Critical Flow Velocities for Involute Parallel Fuel Plate Assemblies," *Transactions of the American Nuclear Society and the European Nuclear Society. 1988 International Conference on Nuclear Fission: Fifty Years of Progress in Energy Security and the Topical Meeting TMI-2 Accident: Materials Behavior and Plant Recovery Technology* 57, 298, TANSAO57 1-548 (1988).

6. E. B. Johannson, "Hydraulic Instability of Reactor Parallel-Plate Fuel Assemblies," Paper No. 57, *Nuclear Engineering and Science Conference*, Engineers Joint Council, April 4–7, 1960.

7. R. J. Scavuzzo, *Hydraulic Instability of Flat Parallel Plate Assemblies*, Ph.D. Dissertation, University of Pittsburgh, 1962.

8. G. E. H. Smissaert, *Hydroelastic Instabilities in Fuel Plate Elements*, Ph.D. Dissertation, Pennsylvania State University, 1966.

9. H. Kraus, *Thin Elastic Shells*, Wiley, New York, 1967.

10. H. C. Schutt, "Losses of Pressure Head Due to Sudden Enlargement of a Flow Cross Section," *Trans ASME*, 51, Part 1, 83–87 (1929).

11. J. K. Vennard, *Elementary Fluid Mechanics*, 317, 4th Ed., Wiley, New York, 1961.

12. J. L. Hobbs, *Pressure Loss Computations in Incompressible Fluid Flow*, 34, APEX-754, General Electric Company, August 1961.

13. L. Collatz, *The Numerical Treatment of Differential Equations*, 30, Springer, Berlin, 1960.

14. B. S. Garbow et al., "Matrix Eigensystems Routines," *EISPACK Guide Extension*, Springer, Berlin, 1977.

15. D. E. Muller, "A Method for Solving Algebraic Equations Using an Automatic Computer," *Mathematical Tables and Other Aids to Computation* **10**, 208–215 (1956).

16. M. P. Paidoussis and N. T. Issid, "Dynamic Stability of Pipes Conveying Fluid," *J. Sound and Vibration*, **33(3)**, 267–294 (1974).

17. C. R. Luttrell, Oak Ridge Natl. Lab., Personal Communication to W. K. Sartory, Oak Ridge Natl. Lab., Jan. 11, 1990.

18. *ADINA, A Finite Element Program for Automatic Dynamic Incremental Nonlinear Analysis*, ADINA Engineering Inc., December 1984.

Internal Distribution

1. C. W. Alexander
2. R. G. Alsmiller
3. J. L. Anderson
4. B. R. Appleton
5. S. H. Buechler
6. N. C. J. Chen
7. G. L. Copeland
8. B. L. Corbett
9. J. M. Corum
10. F. C. Difilippo
11. J. R. Dixon
12. G. F. Flanagan
13. W. R. Gambill
14. M. L. Gildner
15. R. C. Gwaltney
16. R. M. Harrington
17. J. B. Hayter
18. D. T. Ingersoll
19. J. A. Johnson
20. J. E. Jones, Jr.
21. R. A. Lillie
22. C. R. Luttrell
23. J. A. March-Leuba
24. B. S. Maxon
25. B. H. Montgomery
26. R. M. Moon
27. R. K. Nanstad
28. R. E. Pawel
29. F. J. Peretz
30. R. T. Primm, III
31. C. C. Queen
32. A. E. Ruggles
33. T. L. Ryan
34. W. K. Sartory
35. D. L. Selby
36. W. F. Swinson
37. R. P. Taleyarkhan
38. P. B. Thompson
39. K. R. Thoms
40. C. D. West
41. B. A. Worley
42. G. T. Yahr
43. G. L. Yoder
44. A. Zucker
45–46. Laboratory Records (RC)

External Distribution

47. R. R. Fullwood, Brookhaven National Laboratory, Upton, NY 11973.
48. W. F. Manning, U.S. Department of Energy, Oak Ridge Field Office, FEDC, MS-8218, P. O. Box 2009, Oak Ridge, TN 37831-8218
49. J. Marks, Research and Test Reactor Fuel Elements, Babcock and Wilcox Co., P.O. Box 785, Lynchburg, VA 24505.
50. W. T. Oosterhuis, Materials Sciences Division, Office of Basic Energy Science, Office of Energy Research, U. S. Department of Energy, ER-132, Washington, DC 20585.
51. J. M. Ryskamp, Idaho National Engineering Laboratory, P. O. Box 1625, Idaho Falls, ID 83415.

52. J. L. Snelgrove, Coordinator, Engineering Applications, RERTR Program, Argonne National Laboratory, 9700 South Cass Avenue, Argonne, IL 60439.
53. I. Thomas, Director, Materials Science Division, Office of Energy Research, U.S. Department of Energy, ER-13, Washington, D.C. 20585.
54. R. P. Wadkins, Idaho National Engineering Laboratory, P. O. Box 1625, Idaho Falls, ID 84515.
55. D. K. Wilfert, Energy Programs, U.S. Department of Energy, Oak Ridge Field Office, FEDC, MS-8218, P.O. Box 2009, Oak Ridge, TN 37831-8218.
56. R. J. Willard, U.S. Department of Energy, Oak Ridge Field Office, P.O. Box 2001, Oak Ridge, TN 37831.

---

57. Office of Assistant Manager for Energy Research and Development, DOE Oak Ridge Field Office, P.O. Box 2001, Oak Ridge, TN 37831-8600
58-59. Office of Scientific and Technical Information, P.O. Box 62, Oak Ridge, TN 37831